Environmental Sciences Europe

RESEARCH

Open Access

Estimation of greenhouse gas emission factors based on observed covariance of CO_2, CH_4, N_2O and CO mole fractions

László Haszpra[1,2*], Zita Ferenczi[2] and Zoltán Barcza[3,4,5]

Abstract

Background: Covariances among major anthropogenic greenhouse gases were studied during three cold-air pool episodes in the Pannonian Basin to better constrain their emission factors for Europe.

Results: On the base of observed covariance between carbon dioxide, methane, carbon monoxide and nitrous oxide atmospheric dry air mole fraction in a region of the Pannonian (Carpathian) Basin during three cold-air pool episodes in January–February 2017, emission factors relative to carbon dioxide were determined. For the determination of the emission of carbon dioxide, a simple boundary-layer budget model was compiled. The model gave 6.3 g m^{-2} day^{-1} carbon dioxide emission for the footprint area of the measurements on average for the period of the episodes. The 6.7–13.8 nmol μmol^{-1}, 0.15–0.31 nmol μmol^{-1} and 15.0–25.8 nmol μmol^{-1} ratios for CH_4:CO_2, N_2O:CO_2 and CO:CO_2, respectively, correspond to 15.3–31.7 mg m^{-2} day^{-1} methane, 0.9–2.0 mg m^{-2} day^{-1} nitrous oxide and 60.0–103.4 mg m^{-2} day^{-1} carbon monoxide emissions for the region. These values are somewhat higher than the officially reported bottom-up annual national averages for Hungary, which are explained by the winter conditions and intensive domestic heating.

Conclusions: The study indicated the high share of biomass burning in residential heating in rural environment that results in high carbon monoxide emission relative to that of carbon dioxide. It also indicated that the actual emission factor for nitrous oxide may exceed the range given in the guidelines for inventory compilation, which should be taken into account in reporting. It is shown that even a simple boundary-layer budget model might give realistic emission estimation under cool-air pool episodes.

Keywords: Greenhouse gases, Relative emission factor, Boundary-layer budget model, Cold-air pool, Concentration covariance

Background

Any change in the atmospheric budgets of greenhouse gases (GHGs), in the radiative forcing of the atmosphere causes global climate change. The drivers of the changing budgets are the natural and anthropogenic emissions, as well as the feedback processes generated by the climate change itself [1]. For the mitigation of climate change, we have to reduce the anthropogenic emission, if we want to avoid geoengineering. While the anthropogenic emission of carbon dioxide can be estimated with reasonable accuracy from fossil fuel usage and industrial statistics, the emissions of the other major greenhouse gases are known only with significant uncertainty [2]. Any contribution, which can improve the emission estimations, may help the better understanding of the greenhouse gas budget of the atmosphere and its processes, as well as it may help the elaboration of emission control strategies and the checking of their effectiveness. Emission inventory guidelines like [3] cannot exactly specify emission factors for each activity at each location that may distort the

*Correspondence: haszpra.l@gmail.com; haszpra.l@met.hu
[2] Hungarian Meteorological Service, P.O. Box 39, Budapest 1675, Hungary
Full list of author information is available at the end of the article

Springer Open

© The Author(s) 2019. This article is licensed under a Creative Commons Attribution 4.0 International License, which permits use, sharing, adaptation, distribution and reproduction in any medium or format, as long as you give appropriate credit to the original author(s) and the source, provide a link to the Creative Commons licence, and indicate if changes were made. The images or other third party material in this article are included in the article's Creative Commons licence, unless indicated otherwise in a credit line to the material. If material is not included in the article's Creative Commons licence and your intended use is not permitted by statutory regulation or exceeds the permitted use, you will need to obtain permission directly from the copyright holder. To view a copy of this licence, visit http://creativecommons.org/licenses/by/4.0/.

officially reported values, the essential input of the European Union's emission control policy. It is highly desirable to check the suggested emission factors wherever it is possible. In this study, we take advantage of special meteorological situations formed in Central Europe to directly estimate emission factors for greenhouse gases.

There are two main types of methods for the determination of emission. The so-called "bottom-up" approach obtains regional, national or global emissions by multiplying statistical activity data with the appropriate emission factors determined empirically for typical sources, while the so-called "top-down" methods are based on atmospheric concentration measurements [4]. Based on atmospheric concentration measurements, the inverse atmospheric transport models can determine the spatial distribution of the intensity of emission (see e.g., [5–8]), while the boundary-layer budget (BLB) methods can estimate the emission of a region [9, 10]. The boundary-layer budget models can be applied from a single night to a several-days-long episode (see e.g., [11–16]).

The sources of greenhouse gases partly overlap. The ratios of their emissions are characteristic for the source. These substances are rather inert chemically, the atmospheric transport affects them uniformly, and therefore, their ratios do not change during the transport time. As a result, the correlation between their concentrations at a monitoring site gives information on the sources. If the emission of any of the substances is known then that of the others can be calculated from the relationship. The correlation method belongs to the "top-down" ones, and it has been widely used for a long time (see e.g., [17–25]). This method is especially applicable for the estimation of the anthropogenic emission in wintertime when the biological activity and photochemical production providing the natural sources of the major anthropogenically influenced greenhouse gases are low.

During winter high-pressure situation, cold air may pile up in the bottom of topographic basins due to the typically low wind speed and the radiative cooling of the surface characterizing such a meteorological situation. The resulted stable atmospheric stratification may persist for several days when it is called a cold-air pool episode [26]. During such an episode, pollutants emitted at the surface accumulate in the shallow boundary layer due to the limited atmospheric mixing. The rate of the accumulation may be used to estimate their emission. The cold-air pool episodes and their remarkable effect on the local/regional air quality are widely studied in the geographically exposed regions of the world, especially in the Intermountain West region of the United States (see e.g., [26–36]).

Hungary is located in the Pannonian (Carpathian) Basin surrounded by the Carpathian Mountains and by the eastern part of the Alps including the northern Dinaric Alps. These surrounding mountains rise 1000–2000 m above the bottom of the basin, the Pannonian Plain. Taking advantage of three cold-air pool episodes formed in the Pannonian Basin in January–February 2017, and the concentration measurements at the greenhouse gas monitoring station of the Hungarian Meteorological Service, we have estimated the relative emission factors of carbon dioxide (CO_2), methane (CH_4), nitrous oxide (N_2O) and carbon monoxide (CO) based on the observed covariance of CO_2, CH_4, N_2O and CO dry air mole fractions. The values obtained are characteristic for the region and for winter conditions, and they can be incorporated into the emission inventories with these constraints. We have also attempted to estimate the absolute emission by means of a simple boundary-layer budget model.

Although carbon monoxide is only a weak greenhouse gas on its own, but influencing the methane content of the atmosphere through chemical reactions, it is often called as "indirect" greenhouse gas. For simplicity, in this paper, we will also use the term "greenhouse gas" or "GHG" for carbon monoxide. Also for simplicity, we use the term "concentration" for the atmospheric dry air mole fraction actually measured.

Measurements and methods

Greenhouse gas concentration measurements

Hegyhátsál tall-tower greenhouse gas monitoring station of the Hungarian Meteorological Service is located in the western part of the Pannonian Plain (46°57′ N, 16°39′ E, 248 m a.s.l.—Fig. 1) where a TV/radio-transmitter tower owned by Antenna Hungária Corporation is equipped with meteorological sensors and gas analyzers. The monitoring site is located in a fairly flat region, which does not modify the large-scale atmospheric conditions significantly. The prevailing wind directions are the northerly and the southerly ones due to the Alps west of the station. Human habitations in the region of the tower are only small villages (100–400 inhabitants). The nearest one is the single-street village Hegyhátsál, giving the name to the monitoring site, which is located 500–1200 m to the northwest and has only 157 inhabitants. The nearest city is Körmend (11,305 inhabitants), 7 km to the northwest. Larger cities of the region are Zalaegerszeg (58,154 inhabitants, 20 km to the southeast) and Szombathely (78,025 inhabitants, 30 km to the north). The numbers of inhabitants are reported by the Hungarian Central Statistical Office for 1 January 2017 [37]. Local roads carry only low traffic, 300–700 vehicles per day [38]. There is no notable industrial activity in this dominantly agricultural region.

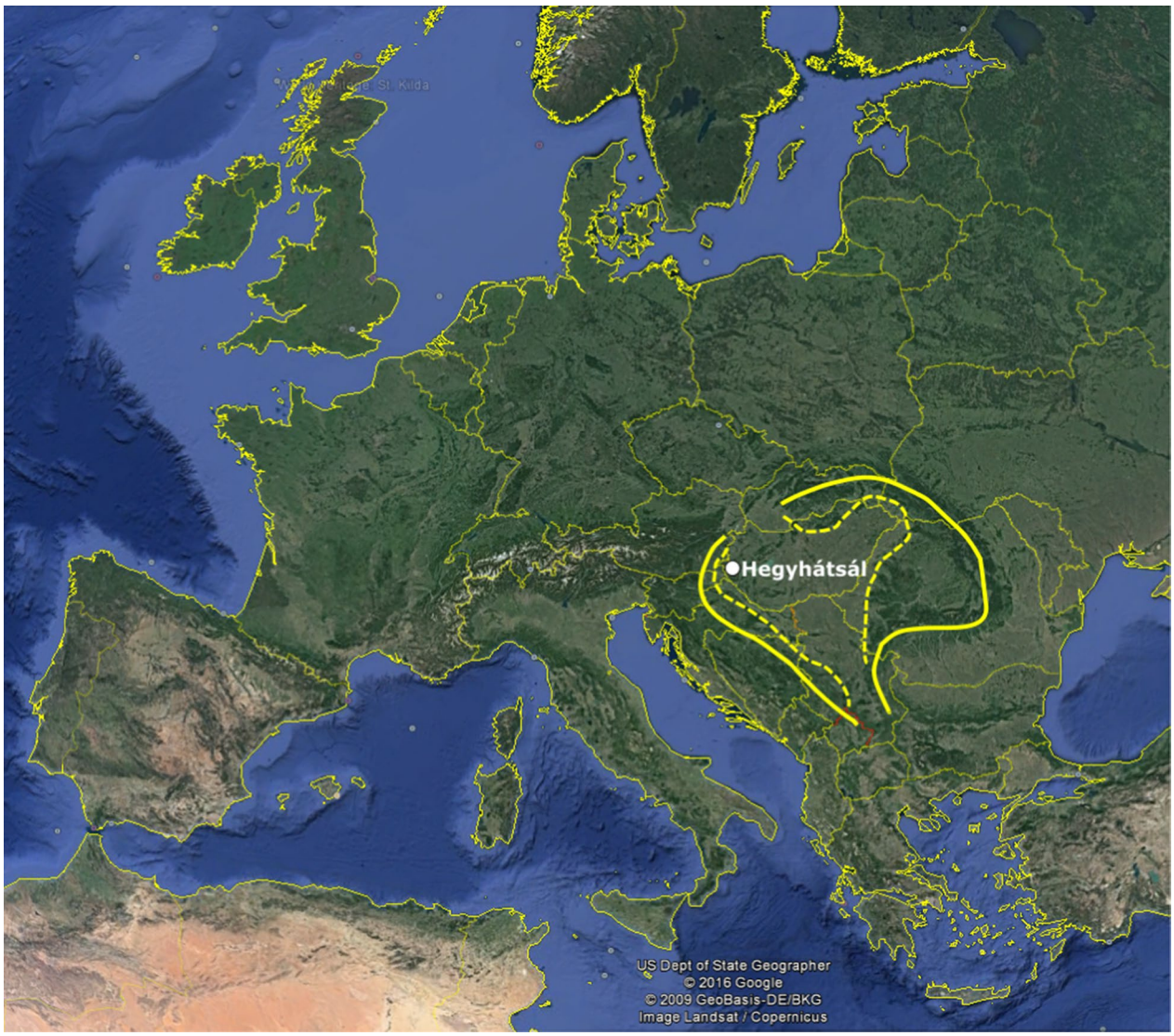

Fig. 1 Location of the monitoring site, the approximate contour of the Pannonian (Carpathian) Basin (solid line) and the Pannonian Plain (dashed line) on Google Earth

At Hegyhátsál tall-tower monitoring site carbon dioxide concentration has been continuously monitored at four elevations (10 m, 48 m, 82 m and 115 m above the ground) since 1994, using non-dispersive infrared gas analyzers (during the period studied here: Model LI-7000, Li-Cor Inc., Lincoln, Nebraska, USA). The analyzer was calibrated against four whole air (CO_2-in-natural-air) standards produced and certified by the Central Calibration Laboratory of the World Meteorological Organization [39]. Carbon dioxide concentration was also measured along with that of methane at 82 m elevation using a Picarro Model G2301 cavity ring-down laser spectrometer (Picarro Inc., Santa Clara, California, USA). At the same elevation nitrous oxide and carbon monoxide concentrations were also monitored by a Model 913-0014 Enhanced Performance N_2O/CO analyzer (Los Gatos Research Ltd., San Jose, California, USA). For CH_4, N_2O and CO measurements the analyzers were calibrated against four whole air standards produced and certified by Max Planck Institute for Biogeochemistry, Jena, Germany. These standards are also traceable to the WMO primary standards. Hegyhátsál tall-tower GHG monitoring site is a member of the Global Atmosphere Watch program of WMO [40] and a member of the Cooperative Global Air Sampling Network operated by the United States National Oceanic and Atmospheric

Administration (NOAA, USA) Earth System Research Laboratory [41]. The station identification code of Hegyhátsál is HUN in both networks.

In addition to the in situ measurements, a pair of flask air samples are taken for NOAA for greenhouse gas measurements every week in the early afternoon hours when the atmospheric mixing is the most intensive. Comparison of the in situ measurements with the flask sample analyses is an integral part of the quality assurance protocol of the station. The surface–atmosphere exchange of CO_2, N_2O and CO is also measured at the site using the eddy covariance method. The sensors are located at 82 m above the ground providing more extended spatial representativeness than the more common low elevation (few meters above the ground) systems. A detailed description of the site, monitoring program, source area characterization and instrumentation can be found in [42–46].

Meteorological data

For the characterization of the weather conditions at the monitoring site, the ERA5 reanalysis dataset of the European Centre for Medium-Range Weather Forecasts [47] was used. Vertical profile of temperature, relative humidity, wind speed and geopotential up to 700 hPa, as well as boundary-layer height, precipitation amount and surface pressure data were downloaded for the grid-point nearest to the monitoring site and for the eight surrounding grid-points (see Fig. 2) with a 0.25° spatial and 1 h temporal resolutions for January–February 2017.

For the identification of the air masses arriving at the monitoring site, the Hybrid-Single Particle Lagrangian Integrated Trajectory (HYSPLIT) Model [48] developed by the US National Oceanic and Atmospheric Administration's Air Resources Laboratory [49] was applied. 3-Dimensional backward trajectories were calculated to trace the air masses back in time for 24 h. The model was fed by the Global Data Assimilation System (GDAS) dataset [50] providing 0.5° spatial and 3-h temporal resolution.

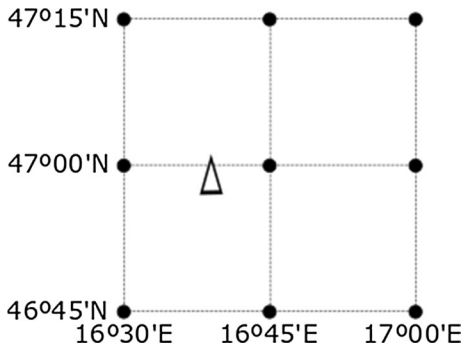

Fig. 2 Location of the monitoring site and the grid-points for which meteorological data from ERA5 dataset were used in the study

Selection of the cold-air pool episodes

The scientific literature is rich in indexes for the identification of stagnant weather conditions favorable for the accumulation of air pollutants (see e.g., [31, 51–57]—and references therein). These indexes comprised different meteorological variables to describe the reduced dispersion processes. The set of identification criteria may include maximum values for wind speed at different elevations, boundary-layer height, ventilation coefficient (integral of the wind speed from the surface to the top of the boundary layer), convective available potential energy, precipitation amount, etc. There is also a criterion on the minimum length of the stagnant period for being considered as an episode. However, there is no universally applicable stagnation index and set of criteria. The best set depends on the properties of the substance studied (e.g., ozone, particular matter, haze, etc.), and it may also depend on the geographical location and season. The threshold values applied as criteria are arbitrary, but supported by previous statistical or phenomenological studies.

Based on previous works [58], in the identification of the cold-air pool episodes, we primarily relied on the value of the boundary layer's convective potential energy usually referred to as shallow convective potential energy (SCP). SCP is formally similar to the convective available potential energy [59], commonly abbreviated as CAPE, but the upper boundary of the integration is fixed at 850 hPa because typically the top of a cold-air pool remains below this level:

$$\mathrm{SCP} = -R_d \int_{p_0}^{850\mathrm{hPa}} \left(T_{\mathrm{vp}} - T_{\mathrm{ve}}\right) \mathrm{d}\ln p,$$

where R_d is the specific gas constant of dry air, p_0 is the surface pressure, while T_{vp} and T_{ve} designate the virtual potential temperatures of the lifted air parcel and that of the environment, respectively. In order to be consistent with the phenomenologically observed cold-air pool episodes, the arbitrarily chosen maximum allowable SCP, ventilation coefficient and surface (10 m) wind speed values for being qualified a day as a stagnation day were −250 J/kg, 3000 m^2/s, and 3 m/s, respectively. We allow only traces of precipitation (< 0.5 mm/day) around the monitoring site during a stagnation episode.

Figure 3 shows the temporal variations of the key meteorological parameters used for the determination of the cold-air pool episodes, and that of a few others characterizing them, for the period of January–February 2017.

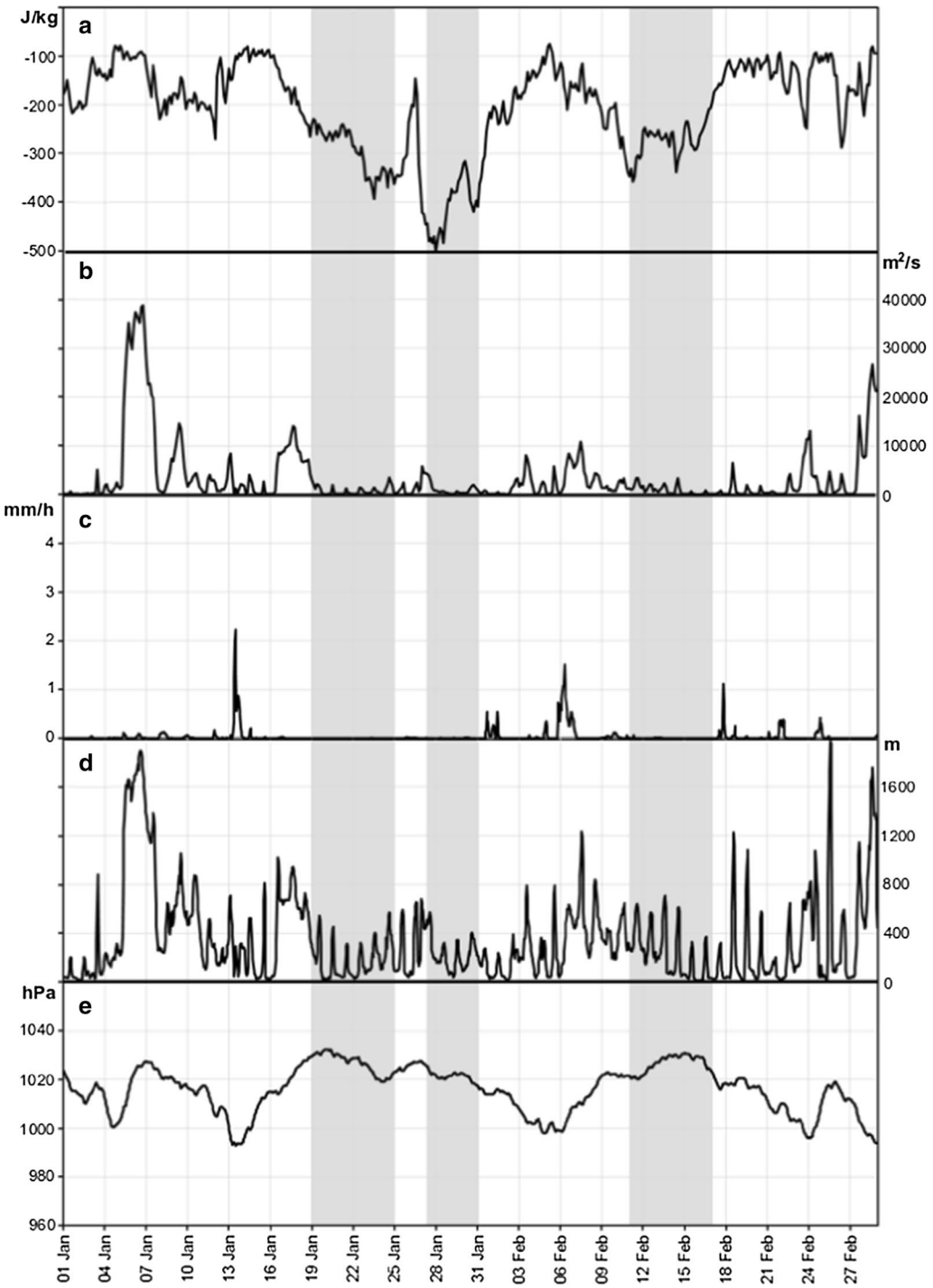

Fig. 3 Temporal variation of SCP (**a**), ventilation coefficient (**b**), hourly precipitation amount (**c**), boundary-layer height (**d**) and sea level pressure (**e**) averaged over the 9 grid-points covered by the study (see Fig. 2), as well as the cold-air pool episodes (gray shaded periods)

After the cold front passed over the Pannonian Basin on 14 January, a stable high-pressure system started developing over Central Europe. By 20 January, it already covered a huge area from the British Islands to the Black Sea with its center in or close to the Pannonian Basin causing gradual cooling in the basin. The system slowly moved to the east, and fresh air entered into the basin from the north at its edge on 24–26 January. The

restrengthened high-pressure system left the region only at the end of January when a small cyclone formed over Western Europe pushed it away to the east. After changeable weather in early February, another persistent high-pressure system developed over Scandinavia and started stretching to the south, over the Pannonian Basin. The cold air accumulated in the basin during this period was swept away by a cold front crossing the region on 17 February.

Figure 3 indicates three cold-air pool episodes (19–24 January, 26–31 January, 11–17 February). The notable meteorological differences among these episodes are in temperature and cloudiness. The second half of January 2017 was unusually cold due to the long-lasting anticyclonic conditions. The daily maximum temperature was always below the freezing point and the minimums were as low as −10 °C. On the contrary, during the episode in February the daily maximum temperature gradually increased up to +10 °C, while the minimums did not go below −4 °C. The radiative cooling was largely balanced by the increasing insolation. The episode at the end of January was heavily foggy, while the other two episodes were mostly clear.

During most of the cold-air pool episodes, air arrived at the monitoring station from the south sector (from southeast to southwest). The only exceptions were the first one and a half days of the first episode in January (19–20 January) and the first day of the episode in February (10 February). Although pollution accumulates all over the basin during stagnation, its distribution is not perfectly uniform due to the weak horizontal mixing. For getting a clearer picture of the emission, we selected only those periods of the cold-air pool episodes when the air arrived from the south sector (20–23 January, 26–31 January, 11–17 February).

Determination of the relative emission factors and the absolute emissions

As the sources of greenhouse gases may partly overlap, the relationship between their emissions can characterize the source or the combination of the sources. The atmospheric transport, dispersion affects the concentration of these chemically inert gases uniformly. The correlation between their concentrations at a monitoring site gives information on the sources. If the emission of any of the substances is known, then that of the others can be calculated from the relationship. However, the correlation method can only provide relative emissions.

We have also attempted to determine the absolute emission, at least on a qualitative level, using a simple boundary-layer budget model. It also checks if such a simple model could provide realistic results under a cold-air pool episode. In this model, three vertically aligned boxes of a unit base area represent the atmosphere: boundary layer, residual layer and the free troposphere (Fig. 4). The height of the lowest box varies with that of the planetary boundary layer. The middle box represents the residual layer. Its height is supposed to be equal with the maximum height of the boundary layer on the previous day and the initial concentration in this box

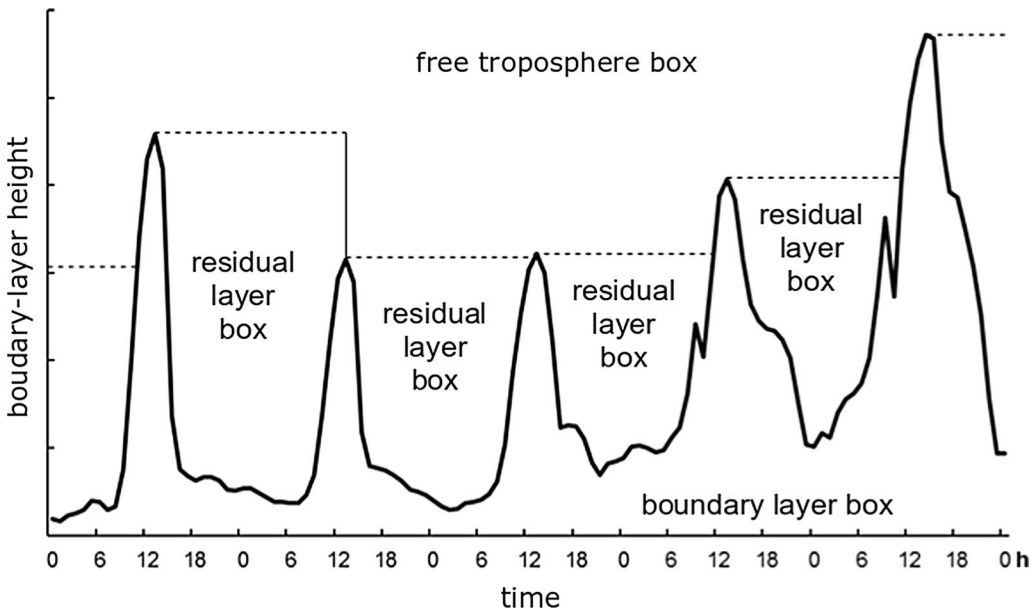

Fig. 4 Structure of the boundary-layer budget model

corresponds to that in the boundary layer at the time of the maximum height. The height of this box and the concentration in it are reset every day when the boundary-layer height reaches its daily maximum. The upper box represents the free troposphere where the concentration is permanently equal with the continental background one. The residual layer is not totally decoupled from the free troposphere. For the simulation of the dilution of the residual layer, its certain portion is replaced with free tropospheric air in each time step. The real vertical exchange of air could only be simulated in a one-dimensional model including the turbulent vertical exchange processes. Assuming a realistic range of 2–4% h^{-1}, we tested the sensitivity of the model to this parameter. The calculated emission varied ± 16% relative to the average in this range. It is not critical besides the other sources of uncertainties with special attention to the neglected variable advection. In the model run presented in this study constant 3% h^{-1} exchange rate between the residual layer and the free troposphere containing background air was used.

The mass balance in a box means that the concentration is driven by the combined effect of the mass leaving and entering the box, while the volume of the box is also changing (see [11, 60, 61]—and references therein). The boundary-layer box receives mass from surface emission and from the residual layer when the height of the boundary-layer is increasing. If the boundary-layer height exceeds the height of the residual layer, the boundary-layer box incorporates mass from the box representing the free troposphere. A part of the mass in the boundary-layer is transferred into the residual layer when the boundary-layer is shrinking, which modifies the concentration in the residual layer. The mixing within both boxes is assumed instantaneous. The concentration in the box representing the free troposphere is kept constant (background concentration).

The surface emission can be calculated so that it maintains the measured concentration change in each time step (1 h). The measurement level on the tower at 82 m above the ground, where all the GHGs are measured, is often above the nighttime boundary-layer, decoupled from the surface, and so the concentration data measured there are not suitable for emission calculations. For the emission estimation, the CO_2 concentration data measured at 10 m above the ground can only be used. This monitoring level was always within the boundary layer. The footprint of the measurements depends on their height above the ground. Therefore, the CO_2 emission calculated on the base of the measurements performed at 10 m above the ground does not fit perfectly into the emission relations determined for the elevation of 82 m, however, the technical and meteorological constraints do not make a more appropriate solution possible. For background concentration, 410 μmol mol^{-1} was set in the model. In January–February 2017, the minimum hourly concentration was 410.94 μmol mol^{-1} at the top of the tower (115 m above the ground), and still it was supposed to be an overestimation of the actual continental background concentration.

Results and discussion

Correlation between the GHG concentrations

Carbon dioxide, methane, nitrous oxide and carbon monoxide have long atmospheric residence time, and so, they undergo the same dispersion and long-range transport. Therefore, the fluctuation of the concentration at a given site is dominated by the emission in the footprint area of the measurements. A high correlation between the concentrations of these gases indicates a common source or a given combination of sources. The slope of the regression line reflects the ratio of their emission strength. Consequently, if the emission of one of the gases is known with reasonable confidence then that of the others can be calculated. Such a "top-down" atmospheric method has already been used for different substances in different parts of the world [19–21, 23].

Figure 5 shows the correlations between the gases studied. The parameters of the regression lines and the correlation coefficients are listed in Table 1. All correlation coefficients are statistically significant at higher than the 99% confidence level.

Figure 5 and Table 1 indicate different emission regimes in the three periods studied: high ratios to CO_2 in the first period (20–23 Jan), the same CO:CO_2 ratio but lower ratios for the other two gases in the second (26–31 Jan), and reduced CO:CO_2 ratio but increased N_2O:CO_2 ratio relative to the previous episode during the last episode (11–17 Feb). Several authors have already reported CO:CO_2 and CH_4:CO_2 ratios from different parts of the world. For N_2O:CO_2 ratio less numerous data are available. The ratios in Table 2 have been selected to reflect the winter season or at least the non-summer one for higher comparability with our measurement results. However, the different climate of the monitoring sites may explain certain differences, and during the period covered by the measurements, there were significant technological developments at certain source categories (see e.g., the evolution of the vehicle exhaust regulations in [62]). Yet, our data fit into the above ranges or they are close to them.

The high CO:CO_2 ratio characterizing the two episodes in January indicates ineffective burning. The relatively high emission of carbon monoxide may originate from domestic heating. This hypothesis is also supported by the temporal variation of emission. In the

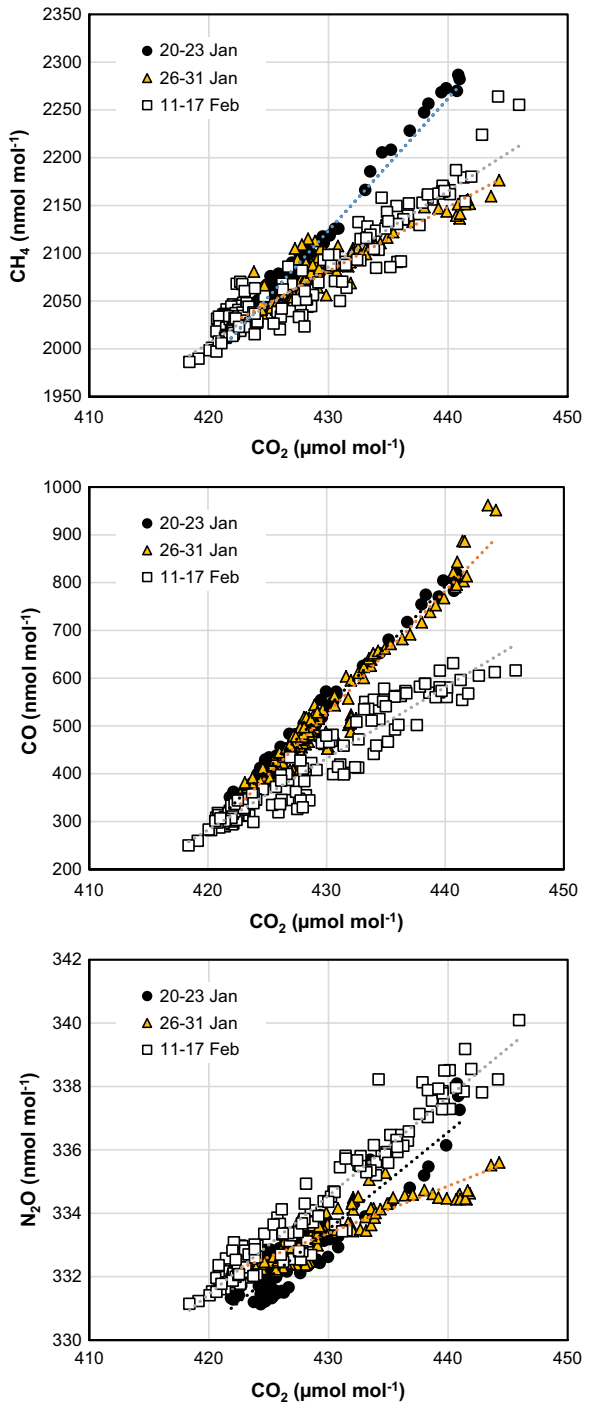

Fig. 5 Covariance between CO_2, CH_4, CO and N_2O concentrations during the episodes

Table 1 Parameter values of the regression lines ($[x] = a[CO_2] + b$), the coefficients of determination (R^2) between CO_2 concentration and the concentration of the other substances measured, as well as the ratio of their standard deviations

	CH_4	CO	N_2O
20–23 Jan			
a [nmol µmol^{-1}]	13.83 ± 0.33	25.59 ± 0.36	0.31 ± 0.01
b [nmol]	− 3821 ± 140	− 10,465 ± 155	202 ± 6
R^2	0.978	0.984	0.864
SD_x/SD_{CO2}	14.13	25.79	0.33
26–31 Jan			
a [nmol µmol^{-1}]	6.69 ± 0.24	25.79 ± 0.59	0.15 ± 0.01
b [nmol]	− 797 ± 105	− 10,563 ± 253	269 ± 3
R^2	0.853	0.937	0.773
SD_x/SD_{CO2}	7.25	26.64	0.17
11–17 Feb			
a [nmol µmol^{-1}]	7.95 ± 0.21	14.96 ± 0.34	0.31 ± 0.01
b [nmol]	− 1333 ± 89	− 6000 ± 143	201 ± 3
R^2	0.897	0.923	0.940
SD_x/SD_{CO2}	8.39	15.57	0.32

case of constant emission, the concentration and the boundary-layer height are anticorrelated. The increasing boundary-layer height helps the dilution of the emitted substances reducing the concentrations, while as soon as the boundary-layer height is decreasing the emission starts increasing the concentrations in it. However, this phenomenon cannot be observed during the episodes in January ($r = 0.18$ and $r = -0.02$, respectively), which suggests a covariance between the emission and the boundary-layer height keeping the concentration virtually independent of the boundary-layer height. In the villages in the region of the monitoring site mostly manually fed traditional, coal- or wood-burning heating appliances are used, although natural gas is also available. People ignite the stoves in the morning and leave them to cool down by the evening resulting in a dominantly morning, noontime emission. The high CH_4:CO_2 and N_2O:CO_2 ratios suggest the dominance of biomass burning. $\Delta^{14}CO_2$ measurements also indicate the high ratio of "modern" carbon in the excess CO_2 in winter [70]. N_2O:CO_2 ratio in the first episode in January, and also in February, is above the upper limit calculated from the IPCC 2006 Emission Guideline [3] for wood/wood waste burning in the residential combustion category (0.15 nmol mol^{-1}; upper value for N_2O emission: 15 kg TJ^{-1} [0.341 kmol TJ^{-1}]; lower value for CO_2 emission: 95,000 kg TJ^{-1} [2159 kmol TJ^{-1}]). The high N_2O:CO_2 ratio may also indicate a contribution from the transport sector, however, the traffic in the region is generally low. This result may have implication in the compilation of the national emission inventory report.

Domestic heating might not play such a dominant role during the episode in February when the temperature

Table 2 CH_4:CO_2, CO:CO_2 and N_2O:CO_2 ratios measured in the different parts of the world during non-summer seasons

Site/region	CH_4:CO_2 nmol µmol^{-1}	N_2O:CO_2 nmol µmol^{-1}	CO:CO_2 nmol µmol^{-1}	References
Arctic, European pollution plume	9.0–15.6		13.1–19.3	[18]
Black Forest, European mountain site	4.8–9.9			[25]
Ireland, western European pollution plume	7.2[a]	0.28[a]		[63]
Ireland	41.3	0.93		[64]
High Tatras, European mountain site	9.5–11.7			[65]
Los Angeles region, California, USA	7.8 ± 0.8	0.5 ± 0.3	11 ± 2	[66]
Irvine, California, USA			6.5–10.0	[67]
Rural site in China, 100 km NW from Beijing			39–75	[21]
South Corea, China			6–39	[68]
Los Angeles region, California, USA	5.3–7.3			[22]
Salt Lake Valley, Utah, USA			7.2–9.4	[27]
Alps, Germany, high mountain site	4.7–7.4		3.5–8.0	[69]
Rural site, Yangtze River Delta, China	5.5–7.5			[23]
Rural site, Pannonian Basin, Europe	6.7–13.8	0.15–0.31	15.0–25.8	This study

[a] Calculated from the CH_4:^{222}Rn, N_2O:^{222}Rn and CO_2:^{222}Rn ratios given in the publication

was significantly higher. The correlation coefficient between the boundary-layer height and the CO_2 concentration at 10 m elevation was −0.58, as it is expected in the case of a temporarily more even emission, and the CO:CO_2 ratio was also lower.

Estimation of the emission

The boundary-layer budget model could only be used for the determination of the carbon dioxide emission because the other gases were measured only at such a high elevation (82 m above the ground) that was above the boundary layer during several nights. The box-model described in "Determination of the relative emission factors and the absolute emissions" section driven by ERA5 boundary-layer height data systematically gave negative emission for 2–4 h after the time of the maximum height. It was the consequence of the decreasing boundary-layer height, while the concentration measured in it was stagnant or still decreasing. It seems that the boundary-layer calculated for ERA5 collapses too early for the given meteorological situations. To overcome this artifact the boundary-layer height was fixed for 3 h after reaching its maximum height. This arbitrary solution largely eliminated the temporary negative emission and resulted in realistic overall emission values. A simple box model can only aspire to provide a qualitative emission estimation. In addition to the arbitrary solution, the advection not considered by the model also contributes to the uncertainty. The calculated CO_2 emissions are 5.3 ± 3.1 g m^{-2} day^{-1}, 8.3 ± 10.8 g m^{-2} day^{-1}, and 8.4 ± 4.9 g m^{-2} day^{-1} for the three episodes, respectively. Uncertainty is given as the standard deviation of the calculated daily emissions during an episode. Emission values are expressed here and throughout the paper in mass of CO_2, CH_4, N_2O, and CO, respectively.

For Hungary, covering the significant portion of the Pannonian Plain, only annual national anthropogenic CO_2 emission data compiled following the IPCC Guideline [3] are available. Emission data at finer spatial and temporal resolutions are not available yet. The reported annual national anthropogenic CO_2 emission for 2017 was 49,646 Gg [71]. It gives 1.46 g m^{-2} day^{-1} for the territory of the country on average. While the intensity of several sources does not show remarkable seasonal variation, the emission of commercial, institutional and residential heating, including biomass burning, responsible for 19,163 Gg in 2017 (0.56 g m^{-2} day^{-1}) is concentrated for the winter season. Assuming that 2/3 of this emission are released into the atmosphere during the coldest 2 months, January and February (12,775 Gg during 59 days, equivalent to 2.33 g m^{-2} day^{-1}), we can estimate (1.46–0.56) + 2.33 = 3.23 m^{-2} day^{-1} anthropogenic emission for these months as a nationwide average. Hegyhátsál tall-tower GHG monitoring station is also the place of continuous surface–atmosphere CO_2 exchange measurements characterizing the net ecosystem exchange of the neighboring, dominantly agricultural region with forest patches [42]. This measurement indicates 2.00 g m^{-2} day^{-1} net release from the biosphere on average for January–February, 2017. Although the footprint of the flux measurements is only of the order of 10 km^2, much smaller than that assumed for the concentration measurements, the resulted value may be valid for an extended region having the same land cover. Adding

up these terms, we can estimate 5.23 g m^{-2} day^{-1} CO_2 emission for an average winter day for Hungary, which is fairly close to the model result based on a few, actually measured days. Of course, we must not forget that the anthropogenic and biospheric emissions are not evenly distributed over the country and the uncertainty of the model results is high.

The CO_2 emission values calculated by the model for the three episodes show neither systematic nor significant differences. Taking into account the notable differences in the uncertainty in the calculated emissions for the episodes, for the calculation of the average emission the inverse-variance weighting method was applied. Accepting the average CO_2 emission calculated in this way (6.30 g m^{-2} day^{-1}) and using the measured GHG to CO_2 ratios the emission ranges for CH_4, N_2O and CO can be estimated for the given geographical region and environmental conditions. The inferred emission ranges for CH_4, N_2O and CO are 15.3–31.7 mg m^{-2} day^{-1}, 0.9–2.0 mg m^{-2} day^{-1}, 60.0–103.4 mg m^{-2} day^{-1}, respectively. The natural sources, including the anthropogenically enhanced natural processes, of CH_4, N_2O and CO are presumably low during wintertime when the biological activity is limited by the low temperature. The concentration of the photochemically produced hydroxyl radical is presumably low and so the chemical reactions may not play a significant role in the formation of the GHG concentrations. Therefore, these values should only be compared to the bottom-up anthropogenic emission estimations. The average annual anthropogenic emission of CH_4, N_2O and CO for a unit area of Hungary in 2017 was 8.9 mg m^{-2} day^{-1}, 0.46 mg m^{-2} day^{-1} and 13 mg m^{-2} day^{-1}, respectively. Taking into account that both the emission data calculated by means of the boundary-layer budget model and those from the bottom-up approach carry high uncertainty, and the bottom-up approach gives annual average nationwide emissions, while the BLB model was applied for a few cold winter days when the heating emission might be extremely high, and for a specific region, the differences do not necessarily mean that the nationwide annual averages are underestimated. However, the significant differences justify further studies.

Two questions have remained open: (1) why was the CH_4:CO_2 ratio two times higher in the first episode of January than during the other two episodes, and (2) why did the N_2O:CO_2 ratio varied virtually independently from the other ratios? In the stagnant weather conditions characterizing the episodes studied, the combination of the trajectories with the gridded emissions from the EDGAR 4.3.2 database [72] has not revealed any characteristic features explaining the observed differences. Were the ratios measured influenced by some sort of episodic emission? Detailed footprint and source apportionment analyses may give the answer in the future, especially if activity data of reasonable temporal and spatial resolution are available.

Conclusions

Taking advantage of cold-air pool episodes in the Pannonian Basin, the ratio of carbon dioxide, methane, nitrous oxide and carbon monoxide emissions were determined giving relative emission factors for these substances. The concentrations show high ($r > 0.88$) correlations indicating a given source or combination of sources during each episode. However, the ratios between the emission strength of GHGs studied varied from episode to episode that could only be partially interpreted on the basis of the available data and modeling tools. We also proved that a simple boundary-layer budget model may be capable of providing realistic emission estimation under these special meteorological conditions, although the uncertainty of the model results is obviously high.

Abbreviations

CO_2: carbon dioxide; CH_4: methane; N_2O: nitrous oxide; CO: carbon monoxide; GHG: greenhouse gas; BLB: boundary-layer budget; WMO: World Meteorological Organization; WMO CCL: World Meteorological Organization Central Calibration Laboratory; GAW: Global Atmosphere Watch; NOAA: National Oceanic and Atmospheric Administration; HYSPLIT: Hybrid-Single Particle Lagrangian Integrated Trajectory; GDAS: Global Data Assimilation System; SCP: shallow convective potential energy; CAPE: convective available potential energy; IPCC: Intergovernmental Panel on Climate Change.

Acknowledgements

The authors gratefully acknowledge the NOAA Air Resources Laboratory for the provision of the HYSPLIT transport and dispersion model website (http://www.ready.noaa.gov) used in this publication. The authors also thank Ákos Horváth, István Ihász, Gábor Kis-Kovács and Klára Tarczay (Hungarian Meteorological Service) for the valuable discussions on emission inventories, data retrieval and boundary-layer dynamics.

Authors' contributions

Concept of the study and writing of the manuscript: LH; trajectory evaluation: ZF; biosphere–atmosphere exchange calculations and critical revision of the manuscript: ZB. All authors read and approved the final manuscript.

Funding

The study was supported by the Hungarian National Research, Development and Innovation Office (K129118), while the measurements were partially sponsored by the National Development Agency (OTKA K109764). Z. Barcza's contribution was partially supported by grant EVA4.0 (CZ.02.1.01/0.0/0.0/16_019/0000803) financed by OP RDE.

Availability of data and materials

Meteorological data used in the study were downloaded from the European Centre for Medium-Range Weather Forecasts where they are publicly available (https://cds.climate.copernicus.eu/cdsapp#!/dataset/reanalysis-era5-land?tab=overview). Carbon dioxide data are publicly available from the World Meteorological Organization World Data Centre for Greenhouse Gases (https://gaw.kishou.go.jp/). Methane, nitrous oxide and carbon monoxide concentration data are available from the corresponding author on request.

Ethics approval and consent to participate

Not applicable.

Consent for publication
Not applicable.

Competing interests
The authors declared that they have no competing interests.

Author details
[1] Research Centre for Astronomy and Earth Sciences, Csatkai Endre utca 6-8, Sopron 9400, Hungary. [2] Hungarian Meteorological Service, P.O. Box 39, Budapest 1675, Hungary. [3] Excellence Center, Eötvös Loránd University, Brunszvik u. 2, Martonvásár 2462, Hungary. [4] Dep. of Meteorology, Eötvös Loránd University, Pázmány P. sétány 1/A, Budapest 1117, Hungary. [5] Faculty of Forestry and Wood Sciences, Czech University of Life Sciences Prague, Kamýcká 129, 165 21 Prague 6, Czech Republic.

Received: 24 August 2019 Accepted: 5 December 2019
Published online: 19 December 2019

References

1. Ciais P et al (2013) Carbon and other biogeochemical cycles. In: Stocker TF, Qin D, Plattner G-K, Tignor M, Allen SK, Boschung J, Nauels A, Xia Y, Bex V, Midgley PM (eds) Climate change 2013: the physical science basis. Contribution of working group I to the fifth assessment report of the intergovernmental panel on climate change. Cambridge University Press, Cambridge, pp 465–570
2. Blanco G et al (2014) Drivers, trends and mitigation. In: Edenhofer O, Pichs-Madruga R, Sokona Y, Farahani E, Kadner S, Seyboth K, Adler A, Baum I, Brunner S, Eickemeier P, Kriemann B, Savolainen J, Schlömer S, von Stechow C, Zwickel T, Minx JC (eds) Climate change 2014: mitigation of climate change contribution of working group III to the fifth assessment report of the intergovernmental panel on climate change. Cambridge University Press, Cambridge, pp 351–411
3. IPCC (2006) 2006 IPCC guidelines for national greenhouse gas inventories—prepared by the National Greenhouse Gas Inventories Programme. In: Eggleston HS, Buendia L, Miwa K, Ngara T, Tanabe K (eds). https://www.ipcc-nggip.iges.or.jp/public/2006gl/
4. Nisbet E, Weiss R (2010) Top-down versus bottom-up. Science 328:1241–1243. https://doi.org/10.1126/science.1189936
5. Patra PK et al (2011) TransCom model simulations of CH_4 and related species: linking transport, surface flux and chemical loss with CH_4 variability in the troposphere and lower stratosphere. Atmos Chem Phys 11:12813–12837. https://doi.org/10.5194/acp-11-12813-2011
6. Thompson RL et al (2014) TransCom N_2O model inter-comparison—part 1: assessing the influence of transport and surface fluxes on tropospheric N_2O variability. Atmos Chem Phys 14:4349–4368. https://doi.org/10.5194/acp-14-4349-2014
7. Bergamaschi P et al (2015) Top-down estimates of European CH_4 and N_2O emissions based on four different inverse models. Atmos Chem Phys 15:715–736. https://doi.org/10.5194/acp-15-715-2015
8. Bergamaschi P et al (2018) Inverse modelling of European CH_4 emissions during 2006–2012 using different inverse models and reassessed atmospheric observations. Atmos Chem Phys 18:901–920. https://doi.org/10.5194/acp-18-901-2018
9. Denmead OT, Raupach MR, Dunin FX, Cleugh HA, Leuning R (1996) Boundary layer budgets for regional estimates of scalar fluxes. Glob Change Biol 2:255–264. https://doi.org/10.1111/j.1365-2486.1996.tb00077.x
10. Bakwin PS, Davis KJ, Yi C, Wofsy SC, Munger JW, Haszpra L, Barcza Z (2004) Regional carbon dioxide fluxes from mixing ratio data. Tellus 56B:301–311. https://doi.org/10.1111/j.1600-0889.2004.00111.x
11. Denzler B, Bogdal C, Kern C, Tobler A, Huo J, Hungerbühler K (2019) Urban source term estimation for mercury using a boundary-layer budget method. Atmos Chem Phys 19:3821–3831. https://doi.org/10.5194/acp-19-3821-2019
12. Grant RH, Omonode RA (2018) Estimation of nocturnal CO_2 and N_2O soil emissions from changes in surface boundary layer mass storage. Atmos Meas Tech 11:2119–2133. https://doi.org/10.5194/amt-11-2119-2018
13. Roest G, Schade G (2017) Quantifying alkane emissions in the Eagle Ford Shale using boundary layer enhancement. Atmos Chem Phys 17:11163–11176. https://doi.org/10.5194/acp-17-11163-2017
14. Stieger J, Bamberger I, Buchmann N, Eugster W (2015) Validation of farm-scale methane emissions using nocturnal boundary layer budgets. Atmos Chem Phys 15:14055–14069. https://doi.org/10.5194/acp-15-14055-2015
15. Wang W, Davis KJ, Cook BD, Yi C, Butler MP, Ricciuto DM, Bakwin PS (2007) Estimating daytime CO_2 fluxes over a mixed forest from tall tower mixing ratio measurements. J Geophys Res 112D:D10308. https://doi.org/10.1029/2006JD007770
16. Zinchenko AV, Paramonova NN, Privalov VI, Reshetnikov AI (2002) Estimation of methane emissions in the St. Petersburg, Russia, region: an atmospheric nocturnal boundary layer budget approach. J Geophys Res 107:D4416. https://doi.org/10.1029/2001jd001369
17. Hansen ADA, Conway TJ, Strele LP, Bodhaine BA, Thoning KW, Tans P, Novakov T (1989) Correlations among combustion effluent species at Barrow, Alaska: aerosol black carbon, carbon dioxide, and methane. J Atmos Chem 9:283–299. https://doi.org/10.1007/bf00052838
18. Conway TJ, Steele LP, Novelli PC (1993) Correlations among atmospheric CO_2, CH_4, and CO in the Arctic, March 1989. Atmos Environ 27A:2881–2894. https://doi.org/10.1016/0960-1686(93)90319-T
19. Lee X, Bullock OR Jr, Andres RJ (2001) Anthropogenic emission of mercury to the atmosphere in the northeast United States. Geophys Res Lett 28:1231–1234. https://doi.org/10.1029/2000gl012274
20. Suntharalingam P et al (2004) Improved quantification of Chinese carbon fluxes using CO_2/CO correlations in Asian outflow. J Geophys Res 109D:D18S18
21. Wang Y, Munger JW, Xu S, McElroy MB, Hao J, Nielsen CP, Ma H (2010) CO_2 and its correlation with CO at a rural site near Beijing: implications for combustion efficiency in China. Atmos Chem Phys 10:8881–8897. https://doi.org/10.5194/acp-10-8881-2010
22. Wong KW et al (2015) Mapping CH4: CO2 ratios in Los Angeles with CLARS-FTS from Mount Wilson, California. Atmos Chem Phys 15:241–252. https://doi.org/10.5194/acp-15-241-2015
23. Huang W et al (2019) Anthropogenic CH_4 emissions in the Yangtze river Delta based on a "Top-Down" method. Atmosphere 10:185. https://doi.org/10.3390/atmos10040185
24. Tohjima Y et al (2014) Temporal changes in the emissions of CH_4 and CO from China estimated from CH_4/CO_2 and CO/CO_2 correlations observed at Hateruma Island. Atmos Chem Phys 14:1663–1677. https://doi.org/10.5194/acp-14-1663-2014
25. Schmidt M, Graul R, Sartorius H, Levin I (1996) Carbon dioxide and methane in continental Europe: a climatology, and ^{222}Radon-based emission estimates. Tellus 48B:457–473
26. Whiteman CD, Zhong S, Shaw WJ, Hubbe JM, Bian X, Mittelstadt J (2001) Cold pools in the Columbia Basin. Weather Forecast 16:432–447. https://doi.org/10.1175/1520-0434(2001)016%3c0432:cpitcb%3e2.0.co;2
27. Bares R et al (2018) The wintertime covariation of CO_2 and criteria pollutants in an urban valley of the Western United States. J Geophys Res 123:2684–2703. https://doi.org/10.1002/2017JD027917
28. Green MC, Chow JC, Watson JG, Dick K, Inouye D (2015) Effects of snow cover and atmospheric stability on winter PM2.5 concentrations in Western U.S. valleys. J Appl Meteorol Climatol 54:1191–1201. https://doi.org/10.1175/jamc-d-14-0191.1
29. Malek E, Davis T, Martin RS, Silva PJ (2006) Meteorological and environmental aspects of one of the worst national air pollution episodes (January, 2004) in Logan, Cache Valley, Utah, USA. Atmos Res 79:108–122. https://doi.org/10.1016/j.atmosres.2005.05.003
30. Silcox GD, Kelly KE, Crosman ET, Whiteman CD, Allen BL (2012) Wintertime PM2.5 concentrations during persistent, multi-day cold-air pools in a mountain valley. Atmos Environ 46:17–24. https://doi.org/10.1016/j.atmosenv.2011.10.041
31. Toro AR, Kvakić M, Klaić ZB, Koračin D, Morales SRGE, Leiva GMA (2019) Exploring atmospheric stagnation during a severe particulate matter air pollution episode over complex terrain in Santiago, Chile. Environ Pollut 244:705–714. https://doi.org/10.1016/j.envpol.2018.10.067
32. Whiteman CD, Hoch SW, Horel JD, Charland A (2014) Relationship between particulate air pollution and meteorological variables in Utah's Salt Lake Valley. Atmos Environ 94:742–753. https://doi.org/10.1016/j.atmosenv.2014.06.012

33. Petkovšek Z (1978) Model for the evaluation of mean emission potential of the air pollution with SO_2 in basins. Archiv für Meteorologie, Geophysik und Bioklimatologie, Serie B 26:199–206. https://doi.org/10.1007/bf02242673
34. Lareau NP, Crosman E, Whiteman CD, Horel JD, Hoch SW, Brown WOJ, Horst TW (2013) The persistent cold-air pool study. Bull Am Meteorol Soc 94:51–63. https://doi.org/10.1175/bams-d-11-00255.1
35. Lyman S, Tran T (2015) Inversion structure and winter ozone distribution in the Uintah Basin, Utah, U.S.A. Atmos Environ 123:156–165. https://doi.org/10.1016/j.atmosenv.2015.10.067
36. Foster CS, Crosman ET, Horel JD, Lyman S, Fasoli B, Bares R, Lin JC (2019) Quantifying methane emissions in the Uintah Basin during wintertime stagnation episodes. Elem Sci Anth 7:24. https://doi.org/10.1525/elementa.362
37. Hungarian Central Statistical Office (2017) Gazetteer of Hungary, 1st January 2017. https://www.ksh.hu/docs/hun/hnk/hnk_2017.pdf. Accessed 21 June 2019
38. Magyar Közút (2017) Az országos közutak 2016. évre vonatkozó keresztmetszeti forgalma http://internet.kozut.hu/lapok/forgalomszamlalas.aspx. Accessed 6 Dec 2017
39. World Meteorological Organization Central Calibration Laboratory http://www.esrl.noaa.gov/gmd/ccl/. Accessed 12 Aug 2019
40. World Meteorological Organization Global Atmosphere Watch http://www.wmo.int/pages/prog/arep/gaw/gaw_home_en.html. Accessed 12 Aug 2019
41. National Oceanic and Atmospheric Administration Earth System Research Laboratory Cooperative Global Air Sampling Network https://www.esrl.noaa.gov/gmd/ccgg/about.html. Accessed 12 Aug 2019
42. Haszpra L, Barcza Z, Davis KJ, Tarczay K (2005) Long term tall tower carbon dioxide flux monitoring over an area of mixed vegetation. Agric For Meteorol 132:58–77
43. Haszpra L, Barcza Z, Hidy D, Szilágyi I, Dlugokencky E, Tans P (2008) Trends and temporal variations of major greenhouse gases at a rural site in Central Europe. Atmos Environ 42:8707–8716. https://doi.org/10.1016/j.atmosenv.2008.09.012
44. Barcza Z, Kern A, Haszpra L, Kljun N (2009) Spatial representativeness of tall tower eddy covariance measurements using remote sensing and footprint analysis. Agric For Meteorol 149:795–807. https://doi.org/10.1016/j.agrformet.2008.10.021
45. Haszpra L et al (2012) Variation of CO_2 mole fraction in the lower free troposphere, in the boundary layer and at the surface. Atmos Chem Phys 12:8865–8875. https://doi.org/10.5194/acp-12-8865-2012
46. Haszpra L, Hidy D, Taligás T, Barcza Z (2018) First results of tall tower based nitrous oxide flux monitoring over an agricultural region in Central Europe. Atmos Environ 176:240–251. https://doi.org/10.1016/j.atmosenv.2017.12.035
47. Copernicus Climate Change Service (2017) ERA5: Fifth generation of ECMWF atmospheric reanalyses of the global climate. Copernicus Climate Change Service Climate Data Store (CDS) https://cds.climate.copernicus.eu/cdsapp#!/home. Accessed 30 Oct 2018
48. Hybrid-Single Particle Lagrangian Integrated Trajectory (HYSPLIT) Model. https://www.ready.noaa.gov/HYSPLIT_traj.php. Accessed 10 Feb 2018
49. Stein AF, Draxler RR, Rolph GD, Stunder BJB, Cohen MD, Ngan F (2015) NOAA's HYSPLIT atmospheric transport and dispersion modeling system. Bull Am Meteorol Soc 96:2059–2077. https://doi.org/10.1175/bams-d-14-00110.1
50. Kanamitsu M (1989) Description of the NMC global data assimilation and forecast system. Weather Forecast 4:335–342. https://doi.org/10.1175/1520-0434(1989)004%3c0335:dotngd%3e2.0.co;2
51. Holzworth GC (1967) Mixing depths, wind speeds and air pollution potential for selected locations in the United States. J Appl Meteorol 6:1039–1044. https://doi.org/10.1175/1520-0450(1967)006%3c1039:mdwsaa%3e2.0.co;2
52. Korshover J, Angell JK (1982) A review of air-stagnation cases in the eastern United States during 1981—annual summary. Mon Weather Rev 110:1515–1518. https://doi.org/10.1175/1520-0493(1982)110%3c1515:aroasc%3e2.0.co;2
53. Horton DE, Harshvardhan Diffenbaugh NS (2012) Response of air stagnation frequency to anthropogenically enhanced radiative forcing. Environ Res Lett 7:044034. https://doi.org/10.1088/1748-9326/7/4/044034
54. Cai W, Li K, Liao H, Wang H, Wu L (2017) Weather conditions conducive to Beijing severe haze more frequent under climate change. Nat Clim Chang 7:257. https://doi.org/10.1038/nclimate3249
55. Feng J, Quan J, Liao H, Li Y, Zhao X (2018) An air stagnation index to qualify extreme haze events in Northern China. J Atmos Sci 75:3489–3505. https://doi.org/10.1175/jas-d-17-0354.1
56. Huang Q, Cai X, Wang J, Song Y, Zhu T (2018) Climatological study of the Boundary-layer air Stagnation Index for China and its relationship with air pollution. Atmos Chem Phys 18:7573–7593. https://doi.org/10.5194/acp-18-7573-2018
57. Wang X, Dickinson RE, Su L, Zhou C, Wang K (2018) PM2.5 pollution in China and how it has been exacerbated by terrain and meteorological conditions. Bull Am Meteorol Soc 99:105–119. https://doi.org/10.1175/bams-d-16-0301.1
58. Szabóné André K, Szépszó G (2015) Using the OpenIFS model to describe weather events in the Carpathian Basin. ECMWF Newslett 16:11
59. Moncrieff MW, Miller MJ (1976) The dynamics and simulation of tropical cumulonimbus and squall lines. Q J R Meteorol Soc 102:373–394. https://doi.org/10.1002/qj.49710243208
60. Griffiths AD, Parkes SD, Chambers SD, McCabe MF, Williams AG (2013) Improved mixing height monitoring through a combination of lidar and radon measurements. Atmos Meas Tech 6:207–218. https://doi.org/10.5194/amt-6-207-2013
61. Pal S, Lopez M, Schmidt M, Ramonet M, Gibert F, Xueref-Remy I, Ciais P (2015) Investigation of the atmospheric boundary layer depth variability and its impact on the 222Rn concentration at a rural site in France. J Geophys Res 120:2014JD022322. https://doi.org/10.1002/2014jd022322
62. European Environmental Agency (2016) EMEP/EEA air pollutant emission inventory guidebook 2016. EEA Report No 21/2016
63. Biraud S et al (2000) European greenhouse gas emissions estimated from continuous atmospheric measurements and radon 222 at Mace Head, Ireland. J Geophys Res 105D:1351–1366. https://doi.org/10.1029/1999JD900821
64. Biraud S et al (2002) Quantification of carbon dioxide, methane, nitrous oxide, and chloroform emissions over Ireland from atmospheric observations at Mace Head. Tellus 54B:41–60. https://doi.org/10.3402/tellusb.v54i1.16647
65. Necki J et al (2003) Six-year record of atmospheric carbon dioxide and methane at a high-altitude mountain site in Poland. Tellus 55B:94–104. https://doi.org/10.1034/j.1600-0889.2003.01446.x
66. Wunch D, Wennberg PO, Toon GC, Keppel-Aleks G, Yavin YG (2009) Emissions of greenhouse gases from a North American megacity. Geophys Res Lett 36:L15810. https://doi.org/10.1029/2009gl039825
67. Djuricin S, Pataki DE, Xu X (2010) A comparison of tracer methods for quantifying CO_2 sources in an urban region. J Geophys Res 115D:D11303. https://doi.org/10.1029/2009JD012236
68. Turnbull JC et al (2011) Atmospheric observations of carbon monoxide and fossil fuel CO_2 emissions from East Asia. J Geophys Res 116:D24306. https://doi.org/10.1029/2011jd016691
69. Ghasemifard H et al (2019) Pollution events at the high-altitude mountain site Zugspitze-Schneefernerhaus (2670 m a.s.l.), Germany. Atmosphere 10:330
70. Major I et al (2018) Temporal variation of atmospheric fossil and modern CO_2 excess at a Central European rural tower station between 2008 and 2014. Radiocarbon 60:1285–1299. https://doi.org/10.1017/rdc.2018.79
71. Hungarian Meteorological Service (2019) National Inventory Report for 1985–2017 Hungary. https://unfccc.int/documents/194931. Accessed 6 June 2019
72. EDGAR 4.3.2. https://edgar.jrc.ec.europa.eu/. Accessed 11 June 2019

Publisher's Note

Springer Nature remains neutral with regard to jurisdictional claims in published maps and institutional affiliations.